Evaluation of SAFT and PC-SAFT EoS for the calculation of thermodynamic derivative properties of fluids related to carbon capture and sequestration

Nikolaos I. Diamantonis[a,b] and Ioannis G. Economou[a,b,*]

[a]Molecular Thermodynamics and Modelling of Materials Laboratory,
Institute of Physical Chemistry,
National Center for Scientific Research "Demokritos",
GR – 153 10 Aghia Paraskevi Attikis, Greece

[b]The Petroleum Institute, Department of Chemical Engineering,
P.O. Box 2533, Abu Dhabi, United Arab Emirates

[*]To whom all correspondence should be addressed at: ieconomou@pi.ac.ae

Abstract

Carbon capture and sequestration (CCS) technology is going to play an important role in the countermeasures for climate change. The design of the relevant processes requires accurate knowledge of primary and derivative properties of various pure components and mixtures over a wide range of temperature and pressure. This paper focuses on the derivative properties of pure components related to CCS. An equation of state (EoS) with strong physical basis is suitable for such calculations. SAFT and PC-SAFT EoS are used to predict these properties, and their performance is evaluated against literature experimental data. The pressure and temperature for the calculations are selected so as to cover an adequate range for the CCS process. EoS predictions are in good agreement with experimental data, with the exception of the critical region where higher deviations are observed.

Keywords: Derivative properties, carbon capture and sequestration, equation of state

For publication to "Energy & Fuels", Revised Manuscript

June 2011

Introduction

The technology of carbon capture and sequestration (CCS) aims at the reduction of greenhouse gas emissions from energy production plants and other industries. It is one of the most highly considered measures to limit the climate change by reducing the accumulation of CO_2 in the atmosphere.[1] Since fossil fuels are predominantly used for energy production, CCS has a good opportunity to play an important role in the environmental control.

Transport is an important linking part in the CCS process (capture – transport – storage) and especially pipeline transport is considered as the most reliable and cost-effective method of all the suggested ones.[2] A thorough risk assessment study is always needed for this part, in order to estimate the effect of a potential rupture on the pipeline and of course lead the design to avoid such incidents. The design of such systems relies heavily on the accurate knowledge of the thermodynamic properties of the fluid. From volumetric to derivative properties, they are all important for the optimum design. The most efficient way of transporting CO_2 is in the supercritical state,[3] although other researchers[4] claim that the transport could be done in the sub-cooled liquid state. Hence, a wide range of conditions should be covered, from supercritical conditions to ambient temperature and pressure,[5] as well as different compositions of the mixture, so as to study the effect of impurities.[6] Although the stream consists of almost pure CO_2 (composition > 90%)[3], other gases may be found, such as SO_2, NO_x, H_2S, H_2, CO, CH_4, N_2, Ar and O_2, depending on the type of the plant and the capture process.[7]

In order to cover these needs in the framework of an engineering project, the available experimental data solely are not enough. In addition, some of the mixtures such as $CO_2 – SO_2$ are very corrosive and, due to this, the experimental data available are very few.[8-10] Equations of state (EoS) are appealing alternative tools to predict the properties in the desired conditions – composition set. Previous investigators had assessed different EoS regarding reliability and performance. For example, Carroll[11, 12] used the Peng-Robinson (PR) and Soave-Redlich-Kwong (SRK) EoS to study the vapor-liquid equilibria (VLE) behavior of CO_2 mixtures with CH_4 and H_2S, while Li and Yan[1, 6] studied the VLE properties of CO_2 mixtures with a wide range of impurities such as CH_4, O_2, H_2S, H_2O, N_2, Ar and SO_2.[1] Due to the large range of conditions, impurities and properties of interest, research in this field has a lot more to offer in the near future.

The EoS that can be used for these calculations are of three types: specialized EoS such as the Span-Wagner EoS[13] for pure CO_2, cubic EoS such as the PR and RK[14-17], and higher order EoS. The latter ones have evolved in recent years as a powerful tool for thermodynamic property calculations. In this work, the Statistical Associating Fluid Theory (SAFT[18-20]) and its widely used modification, Perturbed Chain-SAFT (PC-SAFT[21]), are used. SAFT is an EoS rooted to statistical mechanics and more specifically to Wertheim's first order thermodynamic perturbation theory (TPT1) for associating fluids[22-25]. It was originally proposed in the early 1990's and a number of modifications and extensions were proposed in subsequent years. The most widely used extension is PC-SAFT. A number of reviews[26, 27]concerning these models are available in the literature.

From a scientific standpoint, it is agreed that the prediction of derivative thermodynamic properties is one of the most demanding tests for an EoS.[28] The majority of literature publications related to SAFT and its variations refer to phase equilibria calculations of pure fluids and mixtures while very few studies have been published on derivative properties calculation. The derivative properties can be calculated by analytical expressions directly derived from the mathematical formalism of the SAFT EoS, without the need for numerical solvers. Deviations from experimental data should be attributed to the model inefficiency and parameters' calculation which is usually based on fitting VLE data.[28, 29]

For CCS applications, important thermodynamic properties include vapor pressure, density and various second order thermodynamic properties such as heat capacities, speed of sound, Joule-Thomson coefficients and isothermal compressibility. The calculation of these properties is a great challenge for all kinds of EoS. It is believed though, that EoS with molecular background, such as SAFT-family EoS, may have better performance in this type of calculations because they include all the important molecular contributions.[28, 30]

Previous work on using SAFT-family EoS for the calculation of derivative properties has been done by several research groups, for a variety of families of compounds using different approaches. For example, second order properties for *n*-alkanes were calculated by Lafitte et al. using various versions of SAFT[31], while Llovell et al.[32-34] used the soft-SAFT EoS to calculate derivative properties for some selected mixtures of *n*-alkanes.

The objective of this work is to evaluate the performance of SAFT and PC-SAFT equations of state in predicting the derivative properties of CO_2, H_2S, N_2, H_2O, O_2 and CH_4 that are of interest to CCS technology. The properties calculated and presented are the isobaric and isochoric heat capacities, speed of sound, Joule-Thomson coefficient and isothermal compressibility. The pure component parameters used for these calculations were fitted to VLE data, which is a relatively standard approach. In this way, the predictive capability of the models for these additional properties is thoroughly evaluated.

SAFT and PC-SAFT Equations of State

The SAFT and PC-SAFT EoS are based on rigorous perturbation theory. In perturbation theory, the potential energy of a relative complex molecular fluid can be described as the sum of the potential energy of a simple reference fluid and a perturbation or correction term. Usually, the former term is known accurately and the challenge consists of the description of the perturbation term. Once a suitable perturbation term exists as a function of temperature, density or pressure and composition, then standard thermodynamic expressions can provide all properties of interest.

In this respect, SAFT and PC-SAFT EoS of state are written as summations of residual Helmholtz free energy terms that occur due to different types of molecular interactions of every pure component in the system under study. The residual Helmholtz free energy is equal to the Helmholtz free energy minus the Helmholtz free energy of the ideal gas at the same temperature T and density ρ.

For a system that consists of associating chains, SAFT and PC-SAFT can be expressed as:

$$\begin{aligned}\frac{A^{res}(T,\rho)}{NRT} &= \frac{a^{res}(T,\rho)}{RT} \\ &= \frac{a(T,\rho)}{RT} - \frac{a^{ideal}(T,\rho)}{RT} \\ &= \frac{a^{ref}(T,\rho)}{RT} + \frac{a^{disp}(T,\rho)}{RT} \\ &= \frac{a^{hs}(T,\rho)}{RT} + \frac{a^{chain}(T,\rho)}{RT} + \frac{a^{disp}(T,\rho)}{RT} + \frac{a^{assoc}(T,\rho)}{RT}\end{aligned} \quad (1)$$

where a is the Helmholtz free energy per mole and the superscripts res, ideal, ref, hs, chain, disp and assoc refer to residual, ideal, reference, hard sphere (monomer reference fluid), chain, dispersion and association, respectively. The individual terms are presented below.

The reference fluid in SAFT is the hard sphere fluid. According to Carnahan and Starling,[35] the EoS for hard spheres is:

$$\frac{a^{hs}}{RT} = m\frac{4\eta - 3\eta^2}{(1-\eta)^2} \tag{2}$$

where m is the number of spherical segments in each molecule and η is the reduced density that can be calculated by the expression

$$\eta = 0.74048\rho m v^o \tag{3}$$

In this expression, v^o is the close-packed hard-core volume of the fluid which is evaluated using the temperature-independent soft-core volume, v^{oo}, from the equation:

$$v^o = v^{oo}\left(1 - C\exp\left(-\frac{3u^o}{kT}\right)\right)^3 \tag{4}$$

which has been proposed by Huang and Radosz[20].

In Eq. 4, $\frac{u^o}{kT}$ is the dispersion energy parameter per segment and C is a constant equal to 0.12 (the only deviating compound is hydrogen, for which the value is 0.241).

The interactions for the formation of chains from the monomer hard spheres are modelled according to the equation:

$$\frac{a^{chain}}{RT} = (1-m)\ln\frac{1-0.5\eta}{(1-\eta)^3} \tag{5}$$

which is based on Wertheim's TPT1.

To account for the dispersion forces between the chains, the Alder[36] equation based on molecular simulation of the square-well fluid is used:

$$\frac{a^{disp}}{RT} = m\sum_{i=1}^{4}\sum_{j=1}^{9} D_{ij}\left(\frac{u}{kT}\right)^i\left(\frac{\eta}{0.74048}\right)^j \tag{6}$$

where D_{ij} are universal constants and:

$$\frac{u}{k} = \frac{u^o}{k}\left(1 + \frac{e}{kT}\right) \tag{7}$$

where $\frac{e}{k}$ is an energy parameter with constant value for most of the molecules with the exception of some gases.[20] The three parameters, m, v^{oo} and $\frac{u^o}{k}$, are regressed for every component using experimental data for vapor pressure and saturated liquid density.

The difference between SAFT and PC-SAFT stems from the reference fluid used. In PC-SAFT, the hard chain fluid is chosen over hard sphere. Consequently, the dispersion term in PC-SAFT EoS is:

$$\frac{a^{disp}}{RT} = -2\pi\rho I_1(n,m) m^2 \varepsilon\sigma^3 - \pi\rho m C_1 I_2(n,m) m^2 \varepsilon^2 \sigma^3 \tag{8}$$

where

$$C_1 = \left(1 + Z^{hc} + \rho \frac{\partial Z^{hc}}{\partial \rho}\right)^{-1} \tag{9}$$

and Z^{hc} is the compressibility factor of hard chains. Furthermore,

$$I_1(n,m) = \sum_{i=0}^{6} a_i(m) n^i \tag{10}$$

$$I_2(n,m) = \sum_{i=0}^{6} b_i(m) n^i \tag{11}$$

where a_i and b_i are functions of the chain length and:

$$a_i(m) = a_{0i} + \frac{m-1}{m} a_{1i} + \frac{m-1}{m}\frac{m-2}{m} a_{2i} \tag{12}$$

$$b_i(m) = b_{0i} + \frac{m-1}{m} b_{1i} + \frac{m-1}{m}\frac{m-2}{m} b_{2i} \tag{13}$$

The association term has its roots to Wertheim's TPT1 and the expression for it is:

$$\frac{a^{assoc}}{RT} = \sum_i x_i \left[\sum_{A_i} \left(\ln X^{A_i} - \frac{X^{A_i}}{2} \right) + \frac{1}{2} M_i \right] \tag{14}$$

where M_i is the number of association sites per molecule of species *i* and X^{A_i} is the fraction of molecules of species i that are not hydrogen bonded at site A.The latter can be calculated by a mass balance that results in:

$$X^{A_i} = \left[1 + \sum_j \sum_{B_j} \rho_j X^{B_j} \Delta^{A_i B_j} \right]^{-1} \tag{15}$$

In this equation ρ_j is the molar density of component j , while $\Delta^{A_i B_j}$ is the strength of the bond between two sites A and B , that belong to different molecules i and j .

The expression for the calculation of hydrogen bond strength is:

$$\Delta^{A_i B_j} = d_{ij}^3 g_{ij}\left(d_{ij}\right)^{seg} \kappa^{A_i B_j} \left[\exp\left(\frac{\varepsilon^{A_i B_j}}{kT} \right) - 1 \right] \tag{16}$$

where $\varepsilon^{A_i B_j}$ is the bonding (or association) energy, $\kappa^{A_i B_j}$ is the bonding volume and $d_{ij} = \frac{1}{2}\left(d_{ii} + d_{jj}\right)$ is the average segment diameter.

In this work, the components under consideration were modelled as chain molecules exhibiting the various interactions discussed above. Associating interactions were taken into account between H_2O molecules and between H_2S molecules. More details on the association scheme of H_2O and H_2S is provided later on.

Since the equations of SAFT and PC-SAFT are written in terms of the Helmholtz free energy, they can be used to produce analytical equations for the evaluation of derivative properties. Hence, by taking the derivative functions of the Helmholtz energy with respect to appropriate variables, one can have the expressions for the derivative properties. For the association term, the formalism of Michelsen and Hendriks[37] was used, that results in analytic expressions and thus reduce computational time substantially compared to the original expressions that require a trial-and-error approach. More specifically, the following derivative properties are examined here:

Thermal expansion coefficient $$\alpha = k_T \left(\frac{\partial P}{\partial T} \right)_v \tag{17}$$

Isothermal compressibility coefficient $$k_T^{-1} = \rho\left(\frac{\partial P}{\partial \rho}\right)_T \quad (18)$$

Isochoric heat capacity $$C_v = -T\left(\frac{\partial^2 a}{\partial T^2}\right)_v \quad (19)$$

Isobaric heat capacity $$C_p = C_v + \frac{T\alpha^2}{k_T \rho} \quad (20)$$

Joule-Thomson coefficient $$\mu = T\left(\frac{\partial P}{\partial T}\right)_v - \rho\left(\frac{\partial P}{\partial \rho}\right)_T \quad (21)$$

Speed of sound $$\omega = \sqrt{\frac{C_p}{C_v}\left(\frac{\partial P}{\partial \rho}\right)_T} \quad (22)$$

Results and Discussion

Pure component parameters were fitted to experimental vapor pressure and saturated liquid density data taken from NIST[38]. In Tables 1 and 2, the parameters for SAFT and PC-SAFT are provided together with the percentage average absolute deviation (AAD %) between experimental data and model calculations. Parameter m refers to the number of spherical segments per molecule, with $m = 1$ corresponding to a spherical molecule. In this case, SAFT and PC-SAFT are expected to provide very similar results. In practice, m is one of the model parameters fitted to experimental vapor pressure and saturated liquid density data and its optimum value is larger than one.

Very good correlation of the vapor pressure and liquid density is obtained in all cases. Calculation of liquid and vapor phase thermodynamic properties were performed for all components in the temperature range 80 – 695 K and pressures up to 20 MPa, and compared with experimental data.

Results for the accuracy of the two models to correlate the CO_2 density at subcritical and supercritical conditions are presented in Figure 1. As a first observation, the critical region is the least accurate correlated by both EoS. PC-SAFT provides the relatively best prediction of the critical point with T_c = 309.5 K and P_c = 7.92 MPa, while for SAFT it is: T_c = 315.5 K and P_c = 9.09 MPa. The experimental values are T_c = 304.13 K and P_c = 7.3773 MPa. This is also in agreement with the more accurate prediction of the vapor pressure by PC-SAFT compared to SAFT. The increasing inaccuracy in the critical region, due to the fact that both models are mean-field theories that do not account for critical fluctuations, is also the main reason for the high deviations between experimental data and model predictions for the derivative properties, as it will be explained next. Away from the critical region, both at subcritical and supercritical conditions, calculations are in very good agreement with the experimental data.

In Table 3, a summary of the AAD % between experimental data and EoS predictions for the various properties of all the components examined is provided. On the average, PC-SAFT performs systematically better than SAFT for all the properties, except for the Joule-Thomson

coefficient. In Figures 2 and 3, error contours of SAFT and PC-SAFT EoS predictions are shown for C_p, speed of sound, Joule-Thomson coefficient and isothermal compressibility coefficient of CO_2. The C_p is well described by both equations, but PC-SAFT is giving lower errors. For the calculation of heat capacities, the ideal gas contribution of the fluid is obtained from the NIST database[38] and the residual contribution from the EoS. The locus of the extreme values of C_p close to the critical point is well reproduced, but the values calculated from SAFT are quite higher than the experimental. The accuracy of the calculations of C_p by the two EoS in this work is an improvement compared to earlier works based on a lattice EoS[39] and a cubic EoS[40]. Calculations for C_v from both EoS are within less than 5 % from experimental data for most gases, with an increasing deviation as the critical point is approached. The picture, however, reverts if one focuses on the residual part of C_v (Figure 4 and Table 4). Both models are in qualitative agreement with experimental data, only. In the vicinity of the critical point, the deviation increases and experimental data predict an increase in C_v^{res} as a function of temperature while both SAFT and PC-SAFT predict the opposite trend. Such failure has been reported also by Llovell et al.[29, 33] for other fluids with the soft-SAFT EoS.

The C_p of CO_2 for a single isobar (12 MPa) was studied further in order to identify the effect of residual over the ideal part of the property and the overall accuracy of the models. Calculations and experimental data are presented in Figure 5. Although both models predict experimental data with reasonable accuracy, PC-SAFT is much more accurate over the entire temperature range. In liquid and near-critical conditions, the residual contribution is significant but at high temperatures it becomes less important.

Calculations for the speed of sound are very accurate for both EoS. PC-SAFT deviates from experimental data at most by 3.1 %, while SAFT performs slightly worse (AAD < 8.6 %), as it can be seen in Table 3. From Eq. 22, one can see that ω depends on C_p, C_v and $\left(\frac{\partial P}{\partial \rho}\right)_T$. Consequently, one can argue that there is some cancellation of errors in the ratio of the two heat capacities and the error in ω is mainly governed by the error in $\left(\frac{\partial P}{\partial \rho}\right)_T$.

The Joule-Thomson coefficient is the least accurately predicted property from all properties examined here. The overall AAD rises to 8.6 % for SAFT and 10.1 % for PC-SAFT (Table 3), something that can be explained based on the fact that the Joule-Thomson coefficient depends on two partial derivatives, as it can be seen in Eq. 21 so the error is probably additive. The error is higher close to the points of phase change. At those points, the Joule-Thomson coefficient value changes from negative to very high positive, in a very narrow temperature range. The reason for this inaccuracy may lie in the fact that in those regions there are also abrupt changes in density. This is why, while the pressure increases, the error in Joule-Thomson coefficient decreases, as the density curves become smoother. It is important also to note that for the light gases (CH_4, N_2 and O_2), PC-SAFT is significantly less accurate than SAFT for the prediction of Joule-Thomson coefficient.

The Joule-Thomson inversion curve is an important property for fluids and refers to the conditions where the Joule-Thomson coefficient is zero. The Joule-Thomson inversion curve of CO_2 is presented in Figure 6, and it can be seen that the two equations perform reasonably well over the entire temperature examined.

The last derivative property examined is the isothermal compressibility coefficient, k_T^{-1}. Here also, the agreement of the predictions with the experimental data is very good away from the critical point and coexistence curve, because again, the fluctuations of density cause error in the calculation of $\left(\frac{\partial P}{\partial \rho}\right)_T$ which is used for the calculation of k_T^{-1}.

For O_2, N_2 and CH_4, contour plots for the percentage absolute deviation experimental data and model predictions for representative properties are presented in Figures 7 and 8. In general, the accuracy of the model follows the pattern observed for CO_2, so it decreases close to the critical point and the coexistence curve. The property less accurately predicted is again the Joule-Thomson coefficient. Overall, the properties of three non-polar, spherical molecules O_2, N_2 and CH_4 can be modelled by SAFT and PC-SAFT with high accuracy.

The accuracy of SAFT-based EoS for the prediction of derivative properties of pure fluids has been thoroughly evaluated by Vega and co-workers[29, 33, 34, 41] using Soft-SAFT and by Lafitte et al.[31, 42] using SAFT-VR EoS. The former work focused on *n*-alkanes, *n*-alkenes and 1-alcohols

and their mixtures at subcritical and supercritical conditions while the latter work concentrated on 1-alcohols and 1-alcohol – *n*-alkane mixtures[42] and *n*-alkanes[31]. A direct numerical comparison between calculations with these other SAFT models and calculations presented here is limited since the fluids and conditions examined are not the same. For the case of CH_4, Llovell and Vega[29] reported an AAD % of 1.82 – 3.11 for the speed of sound, 14.9 – 25.3 for C_v and 3.2 – 9.7 for C_p at supercritical conditions (210 – 286 K), while our predictions result in a much lower % AAD for all three properties.

The last part of the analysis refers to explicit account for hydrogen bonding in H_2S and H_2O. Experimental[43] and literature data[44] indicate that H_2S form dimers through hydrogen bonding, thus the one associating site model (1A) proves suitable in this case. However, calculations with the 2 and 4 site models were also performed to explore the accuracy of these other schemes. Calculations of derivative properties with 2 and 4 associating sites were significantly less accurate than calculations using the 1 site model and so only these latter calculations are presented here. The relevant parameters are presented in Tables 1 and 2. The associating model improves only the correlation of saturated liquid density with PC-SAFT while higher deviations are observed for the vapor pressure (both models) and saturated liquid density correlation with SAFT. Similarly, explicit account of association results in marginal improvement of the correlation of some of H_2S derivative properties over the non-associating model. An indicative graph in Figure 9 shows the AAD % of the total C_p of pure H_2S against the experimental data, by using the 1-site model both in SAFT and PC-SAFT.

For modelling H_2O, the popular 4 associating site model (4C) was used that corresponds to two proton donor and two proton acceptor sites. To a first approximation, this is a physically realistic model. However, it does not account for secondary effects such as three-body interactions, etc. Consequently, an attempt was made to use a different associating scheme for H_2O by assuming a proton donor and a proton acceptor site (2B scheme in SAFT terminology). This is a model used for 1-alcohols, although it is often applied for water, as well. Differences between the 2B and 4C association sites are mainly observed in the prediction of derivative properties with SAFT. Cleary, 4C provides lower error in the calculation of vapour pressure and saturated liquid density (Tables 1 and 2) but also it improves the accuracy of the derivative properties as it can be seen in Table 3.

By comparing the accuracy of the models for the various fluids, it becomes clear that for almost all derivative properties, the highest % AAD between experimental data and model predictions corresponds to H_2O. It should be emphasized here that several other parameter sets provided good correlation of the H_2O phase equilibrium, but failed to predict accurately the derivative properties. For example, deviations of up to 40% were obtained for C_p. Consequently, prediction of the derivative properties can be used as an additional test for pure component parameters.

In Figure 10, contour plots for the percentage absolute deviation for C_p of H_2O are presented. Clearly, the 4-site PC-SAFT model results in much more accurate prediction compared to the 4-site SAFT model for the liquid phase properties. However, higher deviations are observed for the vapor phase heat capacity, so that the overall errors from the two models are comparable, as shown in Table 3. Finally, it is known experimentally that the C_p of liquid water H_2O goes through a minimum at constant pressure. At 10 MPa for example, the experimental minimum occurs at 301.5 K and has a value of 74.831 $J/mol \cdot K$. Calculations with SAFT revealed no minimum value, while PC-SAFT predicted a minimum C_p of 71.581 $J/mol \cdot K$ at 367.7 K.

Conclusions

SAFT and PC-SAFT equations of state were applied to six fluids that are of interest to the CCS technology. Their performance was evaluated for the correlation of vapor pressure and saturated liquid density and for the prediction of second derivative thermodynamic properties in a wide range of conditions.

The parameters used for both equations were fitted to VLE data (vapor pressure and liquid density), and subsequently used to predict the second derivative properties accurately, giving low errors, especially away from the critical point. From a physical point of view, as well as applicability in engineering cases, it is important that a single set of parameters can be used for both volumetric and derivative properties. PC-SAFT is shown to be more accurate than SAFT for CO_2 and H_2S, while for the smaller molecules of O_2, N_2 and CH_4, SAFT accuracy is comparable, if not better, to that of PC-SAFT. For spherical molecules (m = 1), PC-SAFT has no advantage over SAFT, as one might expect based on the formulation of the two theories.

Especially for the associating compounds under investigation, namely H_2S and H_2O, some very useful conclusions stem from this study. Taking into account the hydrogen bonding of H_2S does not improve the performance of the models in the correlation of vapor pressure and the prediction of derivative properties. For H_2O, the 4-site associating model results in reasonably good agreement with experimental data for both the SAFT and the PC-SAFT models for all properties examined. In all cases, the Michelsen and Hendriks[37] formulation was used for the associating term that reduces computational time substantially.

The computation cost for the calculations presented here is low, since the derivative properties from SAFT and PC-SAFT are calculated analytically. Thus, the models can be used reliably for a CCS design.

Acknowledgements

The authors acknowledge financial support from the 7th European Commission Framework Program for Research and Technological Development for project “Quantitative failure consequence hazard assessment for next generation CO_2 pipelines” (Project No.: 241346) and from the Petroleum Institute Research Initiation Funding Program for project “An in-house general-purpose simulator for multiscale multiphase flows in heterogeneous porous media for enhanced oil recovery and carbon capture and storage processes”. Also, The Petroleum Institute is acknowledged for a visiting PhD scholarship to NID.

References

1. Li, H.; Yan, J., *Appl. Energy* **2009**, *86*, 826-836.
2. Svensson, R.; Odenberger, M.; Johnsson, F.; Strömberg, L., *Energ. Convers. Manage.* **2004**, *45*, 2343-2353.
3. Forbes, S. M.; Verma, P.; Curry, T. E.; Friedmann, S. J.; Wade, S. M., CCS Guidelines: Guidelines for Carbon Dioxide Capture, Transport, and Storage. *World Resources Institute* **2008**.
4. Zhang, Z. X.; Wang, G. X.; Massarotto, P.; Rudolph, V., *Energ. Convers. Manage.* **2006**, *47*, 702-715.
5. Mohitpour, M.; Golshan, H.; Murray, A., Pipeline Design & Construction: A Practical Approach. *ASME Press* **2007**.
6. Li, H.; Yan, J., *Appl. Energy* **2009**, *86*, 2760-2770.
7. IPCC, IPCC Special Report: Carbon Dioxide Capture and Storage. A Special Report of Working Group III of the Intergovernmental Panel on Climate Change, **2005**.
8. Lachet, V.; de Bruin, T.; Ungerer, P.; Coquelet, C.; Valtz, A.; Hasanov, V.; Lockwood, F.; Richon, D., *Energy Procedia* **2009**, *1*, 1641-1647.
9. Caubet, F., *Z. kompr. Fluess. Gase Pressluft-Ind.* **1904**, *8*, 65.
10. Bluemcke, A., *Ann. Phys. Leipzig* **1888**, *34*, 10-21.
11. Carroll, J. J., *J. Can. Petrol. Technol.* **2002**, *41*, 25-31.
12. Carroll, J. J.; Mather, A. E., *J. Solution Chem.* **1992**, *21*, 607-621.
13. Span, R.; Wagner, W., *J. Phys. Chem. Ref. Data* **1996**, *25*, 1509–1596.
14. Soave, G., *Chem. Eng. Sci.* **1972**, *27*, 1197-1203.
15. Peng, D.-Y.; Robinson, D. B., *Ind. Eng. Chem. Fund.* **1976**, *15*, 59-64.
16. Redlich, O.; Kwong, J. N. S., *Chem. Rev.* **1949**, *44*, 233-244.
17. Patel, N. C.; Teja, A. S., *Chem. Eng. Sci.* **1982**, *37*, 463-473.
18. Chapman, W. G.; Gubbins, K. E.; Jackson, G.; Radosz, M., *Fluid Phase Equilibr.* **1989**, *52*, 31-38.
19. Chapman, W. G.; Gubbins, K. E.; Jackson, G.; Radosz, M., *Ind. Eng. Chem. Res.* **1990**, *29*, 1709-1721.
20. Huang, S. H.; Radosz, M., *Ind. Eng. Chem. Res.* **1990**, *29*, 2284-2294.
21. Gross, J.; Sadowski, G., *Ind. Eng. Chem. Res.* **2001**, *40*, 1244-1260.
22. Wertheim, M. S., *J. Stat. Phys.* **1984**, *35*, 19-34.
23. Wertheim, M. S., *J. Stat. Phys.* **1984**, *35*, 35-47.
24. Wertheim, M. S., *J. Stat. Phys.* **1986**, *42*, 459-476.
25. Wertheim, M. S., *J. Stat. Phys.* **1986**, *42*, 477-492.
26. Economou, I. G., *Ind. Eng. Chem. Res.* **2001**, *41*, 953-962.
27. Müller, E. A.; Gubbins, K. E., *Ind. Eng. Chem. Res.* **2001**, *40*, 2193-2211.
28. Gregorowicz, J.; O'Connell, J. P.; Peters, C. J., *Fluid Phase Equilibr.* **1996**, *116*, 94-101.
29. Llovell, F.; Vega, L. F., *J. Phys. Chem. B* **2006**, *110*, 11427-11437.
30. Kortekaas, W. G.; Peters, C. J.; de Swaan Arons, J., *Fluid Phase Equilibr.* **1997**, *139*, 205-218.
31. Lafitte, T.; Bessieres, D.; Pineiro, M. M.; Daridon, J.-L., *J. Chem. Phys.* **2006**, *124*, 024509(1-16).
32. Llovell, F.; Vega, L. F., *J. Phys. Chem. B* **2005**, *110*, 1350-1362.
33. Llovell, F.; Peters, C. J.; Vega, L. F., *Fluid Phase Equilibr.* **2006**, *248*, 115-122.
34. Llovell, F.; Vega, L. F., *J. Supercrit. Fluid.* **2007**, *41*, 204-216.
35. Carnahan, N. F.; Starling, K. E., *J. Chem. Phys.* **1970**, *53*, 600-603.
36. Alder, B. J.; Young, D. A.; Mark, M. A., *J. Chem. Phys.* **1972**, *56*, 3013-3029.

37. Michelsen, M. L.; Hendriks, E. M., *Fluid Phase Equilibr.* **2001**, *180*, 165-174.
38. Lemmon, E. W.; Linden, M. O.; Friend, D. G., Thermophysical Properties of Fluid Systems. In *NIST Chemistry WebBook, NIST Standard Reference Database Number 69*, Linstrom, P. J.; Mallard, W. G., Eds. National Institute of Standards and Technology: Gaithersburg MD, 20899.
39. Lee, Y.; Shin, M. S.; Kim, H., *J. Chem. Thermodyn.* **2008**, *40*, 1580-1587.
40. Shin, M. S.; Lee, Y.; Kim, H., *J. Chem. Thermodyn.* **2007**, *40*, 688-694.
41. Dias, A. M. A.; Llovell, F.; Coutinho, J. A. P.; Marrucho, I. M.; Vega, L. F., *Fluid Phase Equilibr.* **2009**, *286*, 134-143.
42. Lafitte, T.; Piñeiro, M. M.; Daridon, J.-L.; Bessières, D., *J. Phys. Chem. B* **2007**, *111*, 3447-3461.
43. Lowder, J. E.; Kennedy, L. A.; Sulzmann, K. G. P.; Penner, S. S., *J. Quant. Spectrosc. Ra.* **1970**, *10*, 17-23.
44. Desiraju, G. R.; Steiner, T., The weak hydrogen bond in structural chemistry and biology. *Oxford University Press Inc.***1999**.

Table 1. SAFT parameters for the components studied in this work and AAD % between experimental data and model correlation for vapor pressure and saturated liquid density in the temperature range indicated. H_2S is modeled both as a non-associating and as a single associating site and H_2O as a 2-site and 4-site component.

Component	m	v^{00} (Å^3)	u/k (K)	e/k (K)	ε^{AB}/k (K)	κ^{AB}	AAD (%)		T (K)
							P^{sat}	ρ^{liq}	
CO_2	2.9271	5.710	136.53	40	-	-	0.92	1.84	225 – 301
CH_4	1.0000	21.566	189.82	0	-	-	0.58	1.82	127 – 191
O_2	1.0000	16.056	154.72	0	-	-	1.58	1.32	90 – 154
N_2	1.0000	19.457	123.53	3	-	-	0.43	0.11	73 – 122
H_2S	2.3482	7.801	207.86	10	-	-	1.80	2.11	188 – 370
H_2S (1A)	1.3991	14.887	284.56	1	1081.44	0.0125	2.19	2.76	188 – 370
H_2O (2B)	2.0070	5.098	301.55	1	2355.63	0.1429	1.19	3.08	275 – 640
H_2O (4C)	2.8530	3.304	167.10	1	1634.70	0.3374	1.09	2.38	275 – 640

Table 2. PC-SAFT parameters for the components studied in this work and AAD % between experimental data and model correlation for vapor pressure and saturated liquid density in the temperature range indicated. H_2S is modeled both as a non-associating and as a single associating site and H_2O as a 2-site and 4-site component.

Component	m	σ (Å)	ε/k (K)	ε^{AB}/k (K)	κ^{AB}	AAD (%)		T (K)
						P^{sat}	ρ^{liq}	
CO_2	2.6037	2.555	151.04	-	-	0.49	0.83	217 – 301
CH_4	1.0000	3.704	150.03	-	-	0.33	1.40	127 – 191
O_2	1.1217	3.210	114.96	-	-	0.34	1.80	90 – 154
N_2	1.2053	3.313	90.96	-	-	0.14	1.92	73 – 122
H_2S	1.7163	3.009	224.96	-	-	0.38	1.90	188 – 370
H_2S (1A)	1.4183	3.243	245.49	735.07	0.0111	0.63	0.41	188 – 370
H_2O (2B)	1.9599	2.362	279.42	2059.28	0.1750	1.18	3.92	275 – 640
H_2O (4C)	2.1945	2.229	141.66	1804.17	0.2039	1.98	0.83	275 – 640

Table 3. Summary of AAD % for all the properties calculated from the two EoS. Calculations for components with an asterisk (*) were not used in the calculation of the average.

Component	SAFT AAD (%)						T (K)	P (MPa)
	ρ	k_T^{-1}	C_v	C_p	μ	ω		
CO_2	2.2	5.8	5.9	8.5	16.3	5.1	220 – 500	0 – 20
CH_4	0.1	0.1	0.1	0.3	0.8	0.1	180 – 500	0 – 12
N_2	0.3	0.6	1.0	0.5	4.7	0.7	80 – 500	0 – 12
O_2	0.3	1.0	1.7	1.1	2.7	1.0	80 – 500	0 – 12
H_2S*	1.6	6.2	6.1	6.9	18.5	3.7	190 – 510	0 – 20
H_2S (1A)	1.2	13.4	4.7	9.1	16.3	8.6	190 – 510	0 – 20
H_2O (2B)*	2.4	21.1	14.8	7.8	35.8	18.8	275 – 695	0 – 20
H_2O (4C)	1.8	12.0	13.4	7.3	11.0	8.5	275 – 695	0 – 20
Average	1.0	5.5	4.5	4.5	8.6	4.0		
	PC-SAFT AAD (%)						T (K)	P (MPa)
	P	k_T^{-1}	C_v	C_p	μ	ω		
CO_2	1.0	2.0	4.5	3.5	7.8	2.3	220 – 500	0 – 20
CH_4	0.7	1.6	0.8	1.1	5.5	0.7	180 – 500	0 – 12
N_2	0.8	1.2	1.1	0.9	14.3	1.0	80 – 500	0 – 12
O_2	0.6	1.7	1.3	1.3	8.4	1.1	80 – 500	0 – 12
H_2S*	0.7	3.9	3.3	4.0	8.3	2.3	190 – 510	0 – 20
H_2S (1A)	0.9	4.4	4.4	3.6	11.9	3.1	190 – 510	0 – 20
H_2O (2B)*	2.9	17.2	10.8	5.6	53.6	23.9	275 – 695	0 – 20
H_2O (4C)	1.0	9.8	11.6	9.8	12.4	3.1	275 – 695	0 – 20
Average	0.8	3.5	4.0	3.4	10.1	1.9		

Table 4. Summary of AAD % for C_v^{res} of CO_2 calculated from the two EoS for T = 220 – 500 K.

	C_v^{res} AAD %	
P (MPa)	SAFT	PC-SAFT
0.1	61.8	50.7
1	60.7	47.0
2	65.8	43.5
5	49.6	38.9
8	46.2	38.7
10	44.5	38.7
12	41.7	37.7
15	38.0	36.2
20	30.8	35.5
Average	48.8	40.8

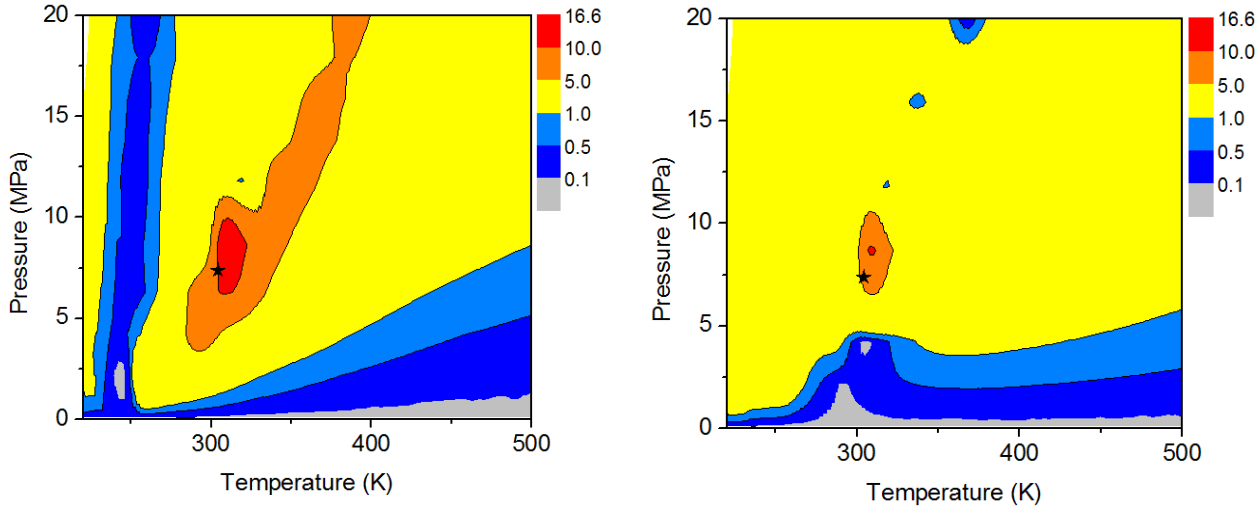

Figure 1. Contour plots of the percentage absolute deviation between experimental data and SAFT predictions (left) and PC-SAFT predictions (right) for the density of pure CO_2. The black star indicates the critical point.

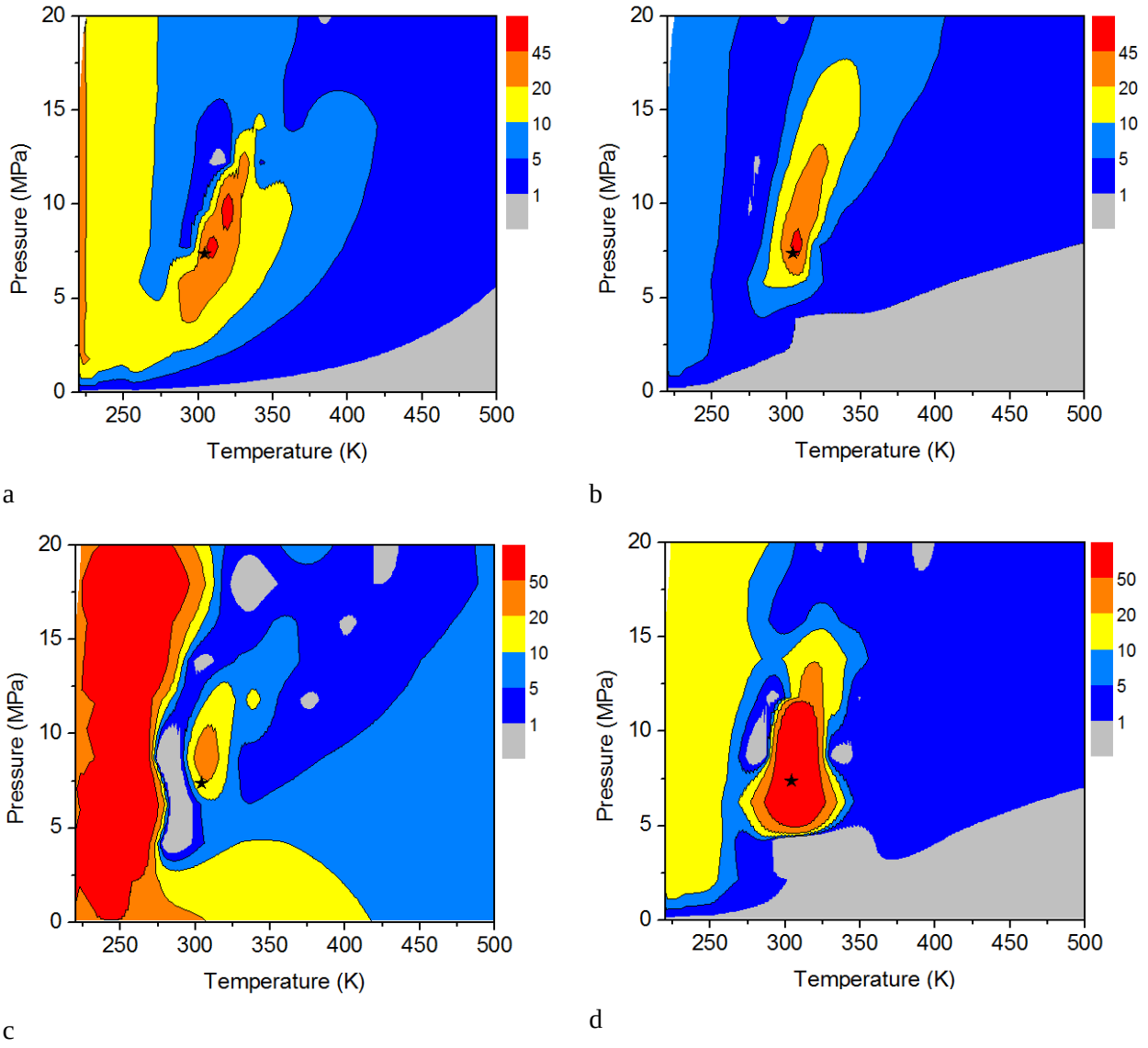

Figure 2. Contour plots of the percentage absolute deviation between experimental data of pure CO_2 and SAFT predictions for: (a) C_p, (b) Speed of sound, (c) Joule-Thomson coefficient and (d) Isothermal compressibility coefficient. The black star indicates the critical point.

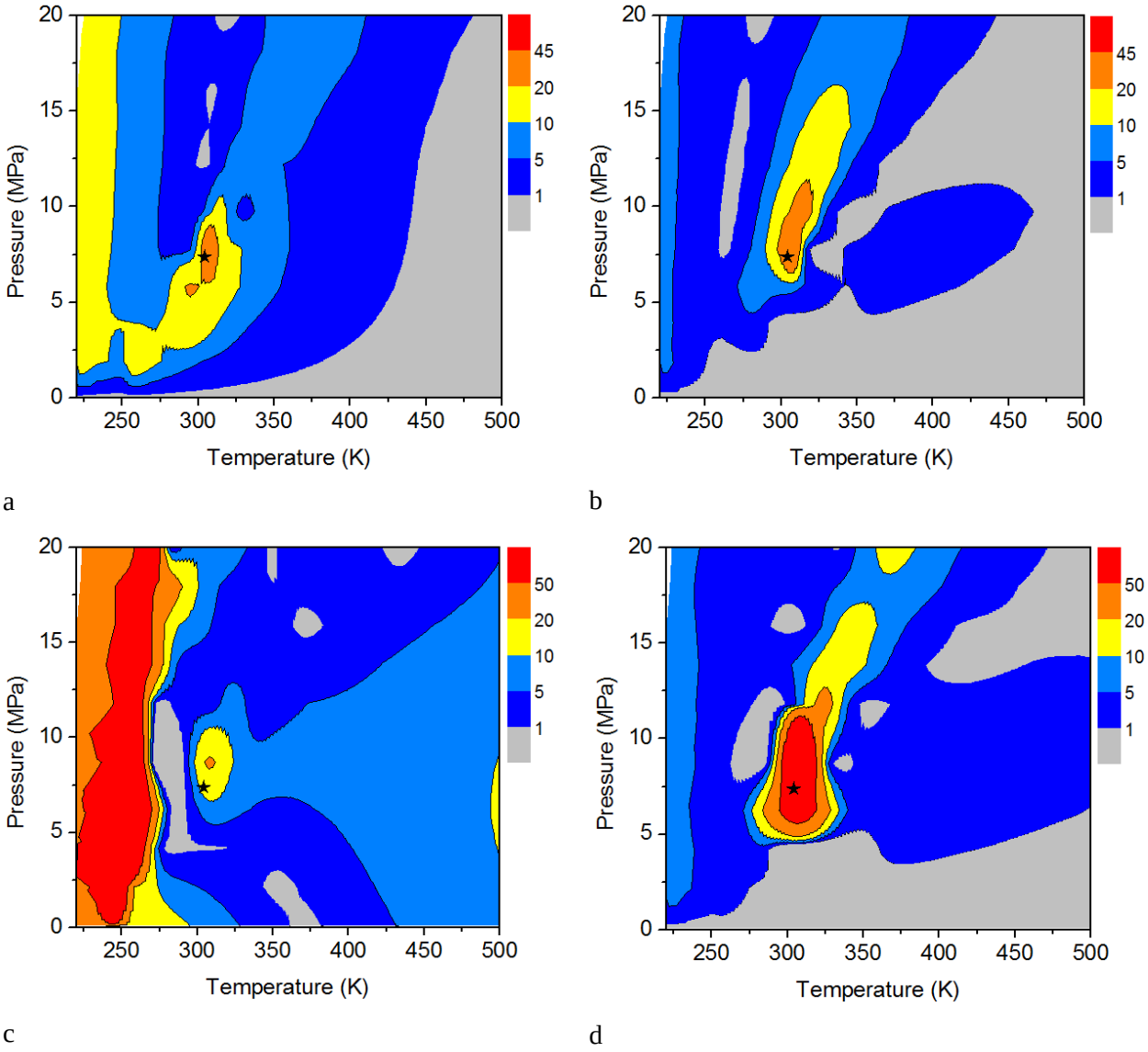

Figure 3. Contour plots of the percentage absolute deviation between experimental data of pure CO_2 and PC-SAFT predictions for: (a) C_p, (b) Speed of sound, (c) Joule-Thomson coefficient and (d) Isothermal compressibility coefficient. The black star indicates the critical point.

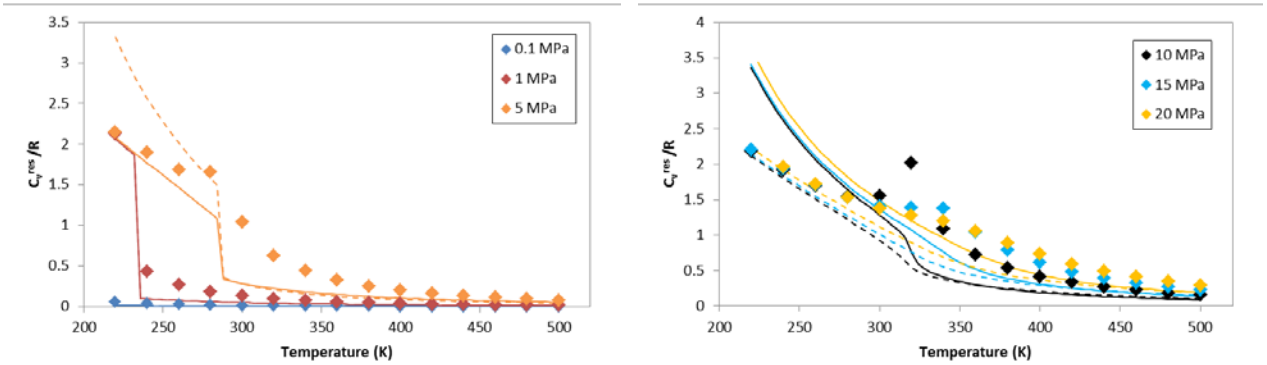

a b

Figure 4. Residual isochoric heat capacity of pure CO_2 for (a) subcritical and (b) supercritical regime. Solid lines are SAFT predictions, dashed lines are PC-SAFT predictions and points are experimental data.[38]

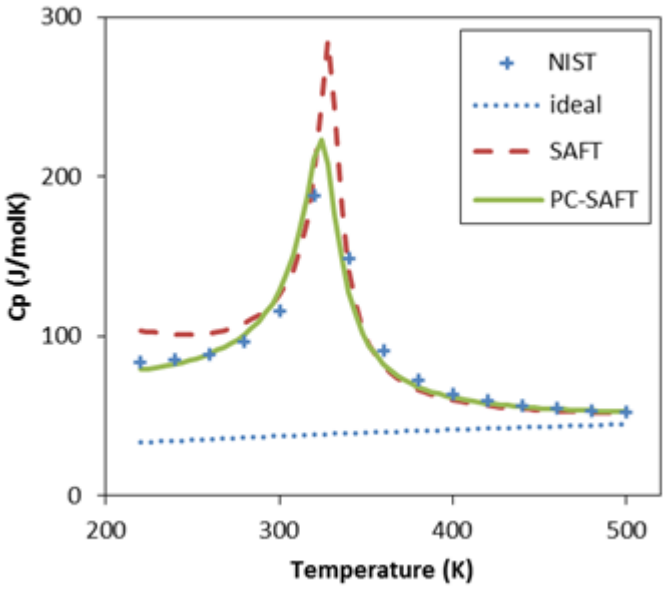

Figure 5. C_p of CO_2 at 12MPa. Experimental data from NIST, ideal gas contribution, SAFT and PC-SAFT predictions.

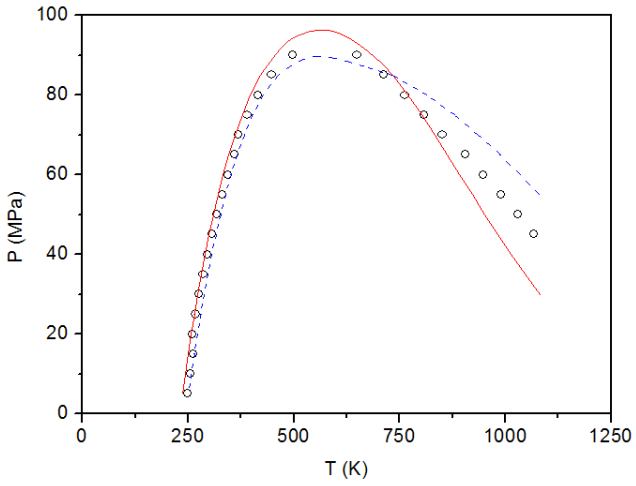

Figure 6. Joule-Thomson inversion curve of pure CO_2. Solid lines are SAFT predictions, dashed lines are PC-SAFT predictions and points are experimental data[38].

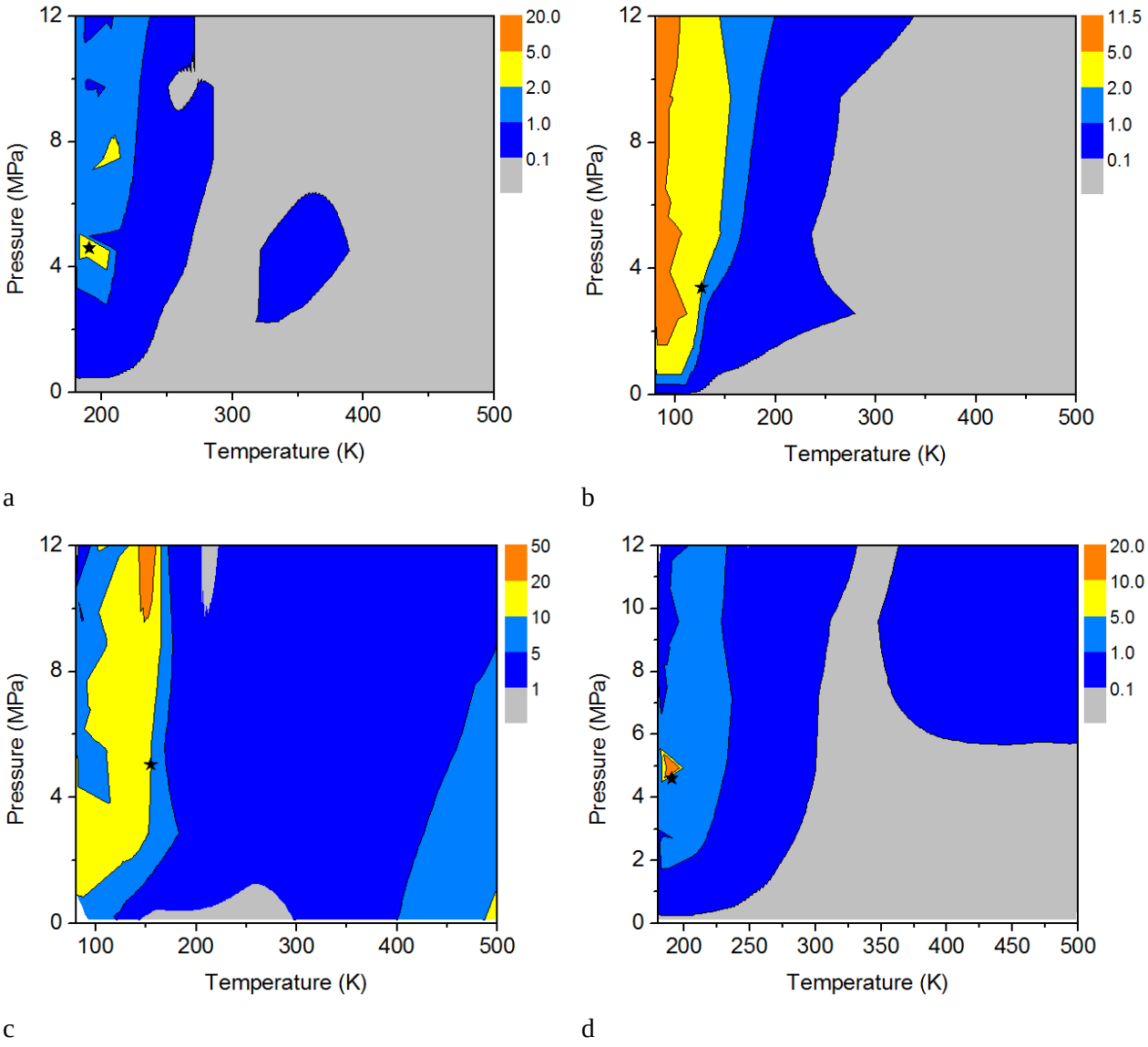

Figure 7. Contour plots of the percentage absolute deviation between experimental data and SAFT predictions for: (a) Isochoric heat capacity of pure CH_4, (b) Speed of sound of N_2, (c) Joule-Thomson coefficient of O_2, and (d) isothermal compressibility coefficient of CH_4. The black star indicates the critical point.

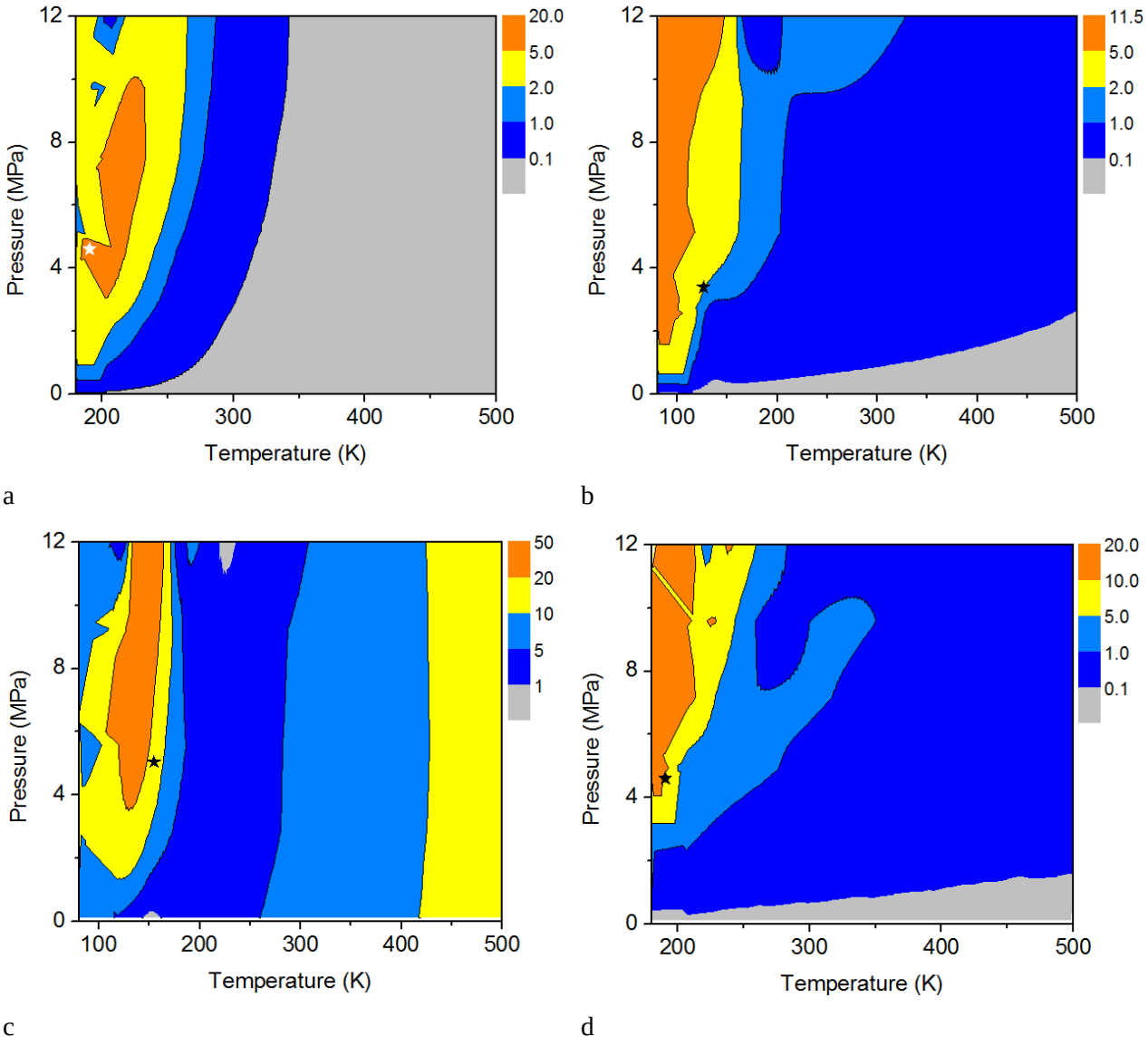

Figure 8. Contour plots of the percentage absolute deviation between experimental data and PC-SAFT predictions for: (a) Isochoric heat capacity of pure CH_4, (b) Speed of sound of N_2, (c) Joule-Thomson coefficient of O_2, and (d) isothermal compressibility coefficient of CH_4. The black star indicates the critical point.

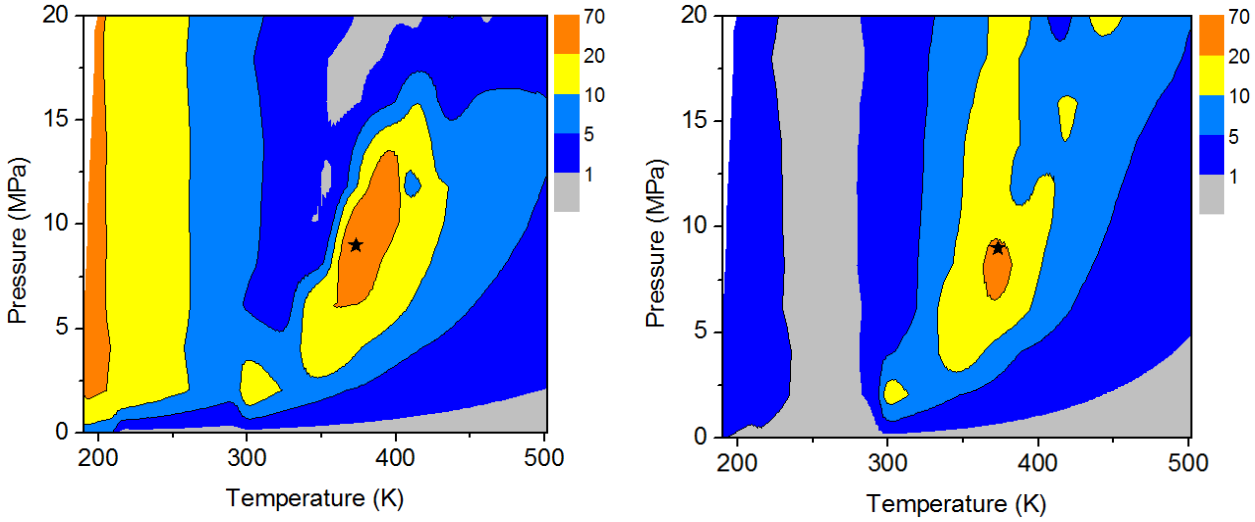

Figure 9. Contour plots of the percentage absolute deviation between experimental data for the C_p of H_2S and predictions from (a) SAFT and (b) PC-SAFT. The black star indicates the critical point.

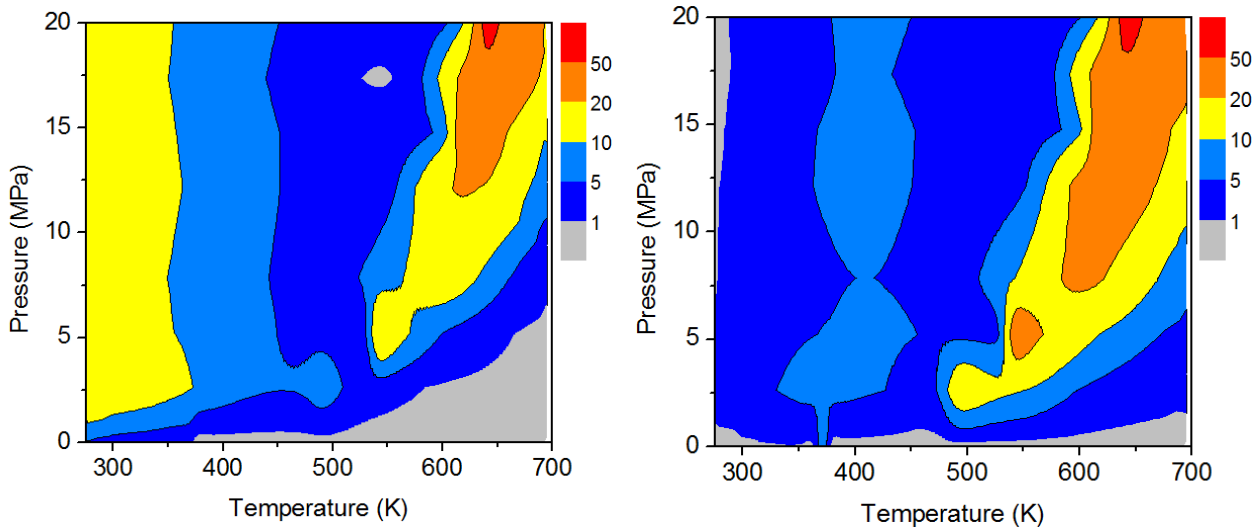

Figure 10. Contour plots of the percentage absolute deviation between experimental data for C_p of H_2O and predictions from (a) SAFT and (b) PC-SAFT. The black star indicates the critical point.